Am J Cancer Res 2025;15(12):5317-5333
www.ajcr.us /ISSN:2156-6976/ajcr0163602

Original Article

Inhibition of ITGB6 stimulates potent anti-tumor responses in immunocompetent mouse models of head and neck squamous cell carcinoma and pancreatic adenocarcinoma

William J MacDonald[1,3,6], Praveen R Srinivasan[1,3,6], Maximilian Pinho-Schwermann[1,3,6], Shengliang Zhang[1,2,3,6], Vida Tajiknia[1,3,6], Connor Purcell[1,6], Jillian Strandberg[1,4,6], Alexis J Lannigan[1,3,6], Wafik S El-Deiry[1,2,3,5,6]

[1]Laboratory of Translational Oncology and Experimental Cancer Therapeutics, The Warren Alpert Medical School, Brown University, Providence, RI 02903, USA; [2]The Joint Program in Cancer Biology, Brown University and The Lifespan Health System, Providence, RI 02903, USA; [3]Department of Pathology and Laboratory Medicine, The Warren Alpert Medical School, Brown University, Providence, RI 02903, USA; [4]Biomedical Engineering Graduate Program, The Warren Alpert Medical School, Brown University, Providence, RI 02903, USA; [5]Hematology-Oncology Division, Department of Medicine, Rhode Island Hospital and Brown University, Providence, RI 02903, USA; [6]Legorreta Cancer Center at Brown University, The Warren Alpert Medical School, Brown University, Providence, RI 02903, USA

Received January 27, 2025; Accepted July 31, 2025; Epub December 25, 2025; Published December 30, 2025

Abstract: *ITGB6*, the gene encoding the β6 subunit of integrin αvβ6, is a potent prognostic marker across multiple cancer types. As a major activator of latent TGFβ and a potent modulator of the tumor immune environment, αvβ6, and consequently, *ITGB6*, has considerable therapeutic implications. *ITGB6* is highly upregulated in squamous cell carcinomas and pancreatic adenocarcinomas, where it disrupts tumor-immune cell signaling. We identify *ITGB6* as a potent clinical prognostic marker of anti-tumor immune response and were able to recapitulate the immune-mediated anti-tumor effect of *ITGB6* in pre-clinical mouse models. Genetic knockout of *ITGB6* in heterotopically-injected head and neck squamous cell carcinoma and pancreatic adenocarcinoma cell lines shows markedly reduced tumor progression and immunogenic cytokine profiles in immunocompetent mice. Additionally, co-cultures of human head and neck squamous cell carcinoma and pancreatic adenocarcinoma with human T-cells show increased T-cell killing upon cancer cell *ITGB6* inhibition. Colony formation experiments give further evidence that the reduced tumor growth observed upon *ITGB6* inhibition *in vivo* is through immunological clearance of cancer cells and not merely through intrinsic factors. Analysis of The Cancer Genome Atlas (TCGA) reveals the high prognostic value of *ITGB6* on overall survival and that high *ITGB6* expression in patients is associated with an inferior response to α-PD-1 and α-PD-L1 immune checkpoint blockade. The potent anti-tumor immune response observed both *in vitro* and *in vivo* upon *ITGB6* inhibition, combined with analysis of RNA-seq data from immune checkpoint blockade-treated patients, encourages the development of ITGB6 blockade and immunotherapy combination regimens. Further pre-clinical studies should facilitate translation of our findings into therapeutic clinical trials for treating immunotherapy-resistant cancers.

Keywords: Integrins, T-cell, cancer, immunotherapy, immune checkpoint blockade, adaptive immunity, TGFβ

Introduction

Immunotherapeutic agents that harness the tumor protective power of the immune system have given new hope to treating cancer types often characterized by treatment resistance and poor prognosis. Immune checkpoint blockade therapy against PD-1 and PD-L1, for instance, has proven effective in a variety of cancers. Lung cancer, metastatic melanoma, genitourinary cancers, and head and neck cancer have shown some susceptibility to PD-1/PD-L1 inhibitors, with effective response rates of 29.03%, 26.91%, 20.66%, and 12.15%

https://doi.org/10.62347/MEAD1055

respectively [1]. Responders will generally experience a duration of response of around one year.

Unfortunately, most patients with these tumor types will see no durable response to immune checkpoint blockade (ICB) therapy. Factors such as immune checkpoint expression, neoantigen burden, immune cell infiltration, and immunosuppressive cytokines in the tumor microenvironment (TME) cause disparate responses to ICB therapy. Among the many targets that are being investigated to interfere with these axes of immune evasion are integrin receptors, which have long been understood to contribute to treatment resistance and immune evasion in cancer [2]. The integrin αvβ6 is of particular interest, as it has been shown to be implicated in tumor protective roles and has proven to be a legitimate immunotherapeutic target in pre-clinical models of colon cancer [3].

αvβ6 is one of 24 transmembrane integrin receptor proteins that facilitate molecular communication between cells and with the ECM. Besides mechanically anchoring cells into the ECM, thus facilitating cell adhesion, integrins serve as mediators of various intracellular and extracellular physiological processes by inducing intracellular transcription factors or activating extracellular molecules for paracrine signaling. As heterodimeric proteins, integrins have an α and a β subunit. Various combinations of the presently identified α and β subunits make up the 24-member integrin family. Integrin αvβ6 plays a powerful and widespread role in cancer biology. αvβ6 is comprised of the αv and β6 subunits, which are encoded by the genes *ITGAV* and *ITGB6,* respectively. While αv complexes with several other β subunits, β6 shows no affinity for other α subunits. Therefore, β6 can be considered the "rate-limiting" subunit for the formation of αvβ6. Consequently, *ITGB6* is generally regarded to be the principal gene responsible for the formation and functioning of αvβ6 [4].

One of the main extracellular functions of αvβ6 is the activation of transforming growth factor-β1 (TGFβ1), which is the member of the TGFβ family most relevant to TME immunosuppression [5]. Integrin αvβ6 contains on its β6 subunit a region that binds the tripeptide arginine-glycine-aspartic acid (RGD) motif found on various cell-surface and extracellular proteins. One of these ligands is the latency-associated protein that forms the latent complex of TGFβ1 that is commonly sequestered in the ECM [6]. Upon binding to αvβ6, active TGFβ1 is released from latency-associated protein and can function as a cytokine in an autocrine or paracrine manner. TGFβ is a widely implicated cytokine that has disparate effects across cell types. However, in the tumor microenvironment, increased TGFβ is associated with immune dysfunction as it has an immunosuppressive effecton T-cells and natural killer cells, resulting in cancer evading the immune system [7]. Decreased local TGFβ around tumors correlates with higher T-cell cytotoxicity [8]. Consequently, TGFβ decreases the effectiveness of immune checkpoint blockade therapy by reducing the infiltration of immune cells into the tumor. Additionally, TGFβ has been shown to drive epithelial-mesenchymal transition (EMT), forcing tumors to a more invasive phenotype with greater metastatic potential [9]. Since αvβ6 is preferentially expressed on various tumor types, blockade of the integrin provides a targeted means of disrupting TGFβ signaling in the TME locally while avoiding the off-target effects inherent to systemic TGFβ blockade [10].

αvβ6 also has potent cell-intrinsic effects such as promoting chemoresistance through an ITGB6-ERK/MAP kinase pathway, whereupon the αvβ6 β-subunit was demonstrated to engage in direct binding to ERK2 [11]. αvβ6 upregulation also appears to be a mechanism of angiogenesis and metastasis in nasopharyngeal carcinoma, through modulation of the FAK pathway [12]. Additionally, recent findings demonstrated yet another immune evasion mechanism of αvβ6 through its role in modulating PF4+ macrophage function and inhibiting response to anti-CD276 ICB [13]. Through its mediation of the tumor microenvironment and the immune system, as well as its cell-intrinsic effects, upregulation of αvβ6 by malignant cells acts upon nearly all cancer hallmarks. Therefore, *ITGB6* is a highly attractive therapeutic target that shows much promise for clinical development.

Materials and methods

TCGA RNA-seq analysis

A Human Protein Atlas query surveyed the upregulation of *ITGB6* across cancer types (**Figure 1A**). Cancer *ITGB6* expression was then compared to expression in paired adjacent nor-

mal tissue using the TNMplot tool on a concatenated set of GEO, GTex, TCGA, and TARGET RNA-seq databases that were normalized according to the DESeq2 pipeline [14, 15] (**Figure 1B**).

Cell culture

Both CAL27 (ATCC, # CRL-2095) and FaDu (ATCC, # HTB-43) head and neck squamous cell carcinoma cells were cultured using high-glucose DMEM medium with L-glutamine (Cytiva, # SH30022.02) with 10% FBS added. HCT116WT (ATCC, # CCL-247) and Capan-2 (ATCC, # HTB-80) cells were cultured using high glucose McCoy's 5A with L-glutamine (Cytiva, # SH30200.FS) and 10% FBS. TALL-104 (ATCC, # CRL-11386) cells were cultured with RPMI-1640 medium with L-glutamine (Cytiva, cat # SH30027.LS) with 20% FBS and IL-2 (Miltenyi, # 130-097744) added as per ATCC guidelines. The cell lines were kept in a 5% CO_2 incubator at 37 degrees Celsius. CT-26 (ATCC, # CRL-2638), CAL27, FaDu, Capan-2, and HCT116WT were obtained from the American Type Culture Collection. MOC1 (Sigma Aldrich, # SCC469) and MOC2 (Sigma Aldrich, # SCC470) cells were obtained from Sigma-Aldrich, and KPCY from Kerafast. Human cell lines were authenticated by short tandem repeat profiling. Mycoplasma infection testing was performed on all cell lines.

Flow cytometry of cell lines

The human cell lines HCT116WT, Capan-2, FaDu, and CAL27 were screened via flow cytometry using an APC-conjugated human ITGB6 antibody (R&D Systems, # FAB4155A). The mouse cell lines CT26, MOC1, MOC2, and KPCY were screened using a mouse/human reactive ITGB6 antibody (Abcam, # ab77906) incubated with an Alexa Fluor 647 conjugated IgG secondary antibody (Thermo Scientific, # A-31571). Cells were gated on singlets, and dead cells were excluded using a Zombie Green cell death dye (BioLegend, # 423111).

CRISPR knockout of ITGB6

Knockout of *ITGB6* was performed by transfection of Alt-R S.p. Cas9-GFP V3 (ID Technology, # 10008100) and single guide RNAs with Lipofectamine CRISPRMAX transfection reagent (Thermo Scientific, # CMAX00003). Single guide RNAs for human *ITGB6* were KO-1: GCTAATATTGACACACCTGA and KO-2: CCTGGCTATTCTTCTCATCG. Single Guide RNAs for mouse *ITGB6* were KO-1: GCTAATATTGACACACCTGA and KO-2: CGTCATCCATAGAGGCGGAG. The non-targeting sequence was CTRL: GAGCTGGACGGCGACGTAAA.

Western blotting

Cells were harvested from 6-well plates after CRISPR knockout and lysed in RIPA buffer (Sigma-Aldrich, # R0278) with a protease inhibitor cocktail (Sigma-Aldrich, # 04693159001). Cells were centrifuged for 20 min at 16,000×g at 4 degrees Celsius. The supernatant was harvested, and a BCA assay (Thermo Scientific, # 23225) was used to measure the protein concentration in the samples. Samples were prepared at a 4X concentration loading buffer (Thermo Scientific, # NP0008) with 10% β-mercaptoethanol. The samples were then boiled at 95 degrees Celsius for 10 min and loaded at 20 µg per lane in 1.0 mm, 12% Bis-Tris, Protein Gels (Thermo Scientific, NP0343BOX). A transfer to PVDF membranes was performed after running the samples along the gel. Membranes were blocked using 5% milk, after which incubation with primary antibodies was performed. CRISPR knockout was verified using western blot ITGB6 antibodies for human (R&D Systems, # MAB41551) and mouse (R&D Systems, # AF2389) cell lines, respectively. Equal loading of samples was ensured across all samples using a loading control antibody for β-actin (R&D Systems, MAB8929). A mouse-reactive secondary antibody (Thermo Scientific, # 31430) was used for β-actin and human ITGB6 antibodies, and a goat-reactive secondary antibody (Thermo Scientific, # 31402) was used for the mouse ITGB6 primary antibody. The blots were visualized using ECL western blotting substrate (Thermo Scientific, # 32106) and a Syngene Imager (RRID: SCR_015770).

Colony formation assays

Colony formation assays were performed in 6-well plates for the human cell lines and 12-well plates for mouse cell lines over a 10-day period. CAL27 and FaDu cells were plated at a density of 300 cells per well, while MOC1 and KPCY cells were plated at 200 cells per well. After ten days in culture, the cells were

fixed using 10% formaldehyde for 10 minutes and stained using 0.01% (w/v) crystal violet for 30 minutes. Plates were imaged using a Syngene imaging system (RRID: SCR_015770), and colonies were counted using ImageJ software if they were greater than 50 cells in size. The average of three replicates was calculated.

Cancer and immune cell co-culture

The generated CRISPR *ITGB6* knockout, and respective control cells of CAL27 and FaDu head and neck squamous cell carcinoma, as well as Capan-2 pancreatic adenocarcinoma cell lines were labeled with the fluorescent dye CMFDA (Thermo Scientific, # C2925) and plated at a density of 10,000 cells per well in black, clear-bottom 96-well plates (Greiner, # 655090). After the cells had been allowed to adhere overnight, they were treated with 10 ng/ml of Latent TGFβ (R&D Systems, # 299-LT-005/CF). Subsequently, CMAC (Thermo Scientific, # C2110) fluorescently labeled, nonadherent TALL-104 cells were added to the culture, also at a density of 10,000 cells per well, with ten replicates. The experiment contained both co-culture conditions and tumor cells alone for both *ITGB6* knockout and control cells. Additionally, the cell death marker Zombie Yellow (BioLegend, # 423103) was added to the culture before imaging. The cells were imaged at 24 hours at 20× magnification using a Molecular Devices ImageXpress Confocal HT.ai fluorescent plate reader (**Figure 2F-H**). Cell counts of cancer cells and T cells, as well as the percentage of cancer cells and T cells that were dead, were quantified using colocalization of the respective cell dye and the cell death marker fluorescent channels using the Molecular Devices software (**Figure 2I-T**).

In vivo studies

C57BL/6 mice were obtained from Jackson Laboratories (Nashville, TN) and were housed in a BSL-2 pathogen-free facility. Mice were 14 weeks old at the beginning of the in vivo study. Mice received subcutaneous flank injections of either 1.5×10^6 MOC1 CTRL or MOC1 ITGB6 KO-1 cells or 1.5×10^5 KPCY CTRL or KPCY ITGB6 KO-1 cells. Cancer cells across the KPCY and MOC1 cohorts were diluted to be volumetrically equal and injected at a 1:1 ratio with Matrigel (Corning, # 356231) for a total injected volume of 200 µL. Each of the four cohorts included ten mice at an equal male-to-female ratio. Tumor volumes were measured starting at day five post-injection (**Figure 3F**, **3H**). Tumor volume was recorded according to the formula, tumor volume = (length × width^2)/2, where width is the smaller of the two dimensions. Mice were weighed and their tumor volumes were measured until day 25 post-injection, when the mice were euthanized, and their tumors and organs were harvested. Tumors that did not reach a total volume of 100 mm^3 by the final day were excluded from the analysis. Tumors were surgically removed and gently washed before being weighed (**Figure 3G**, **3I**).

Luminex cytokine profiling of tumor interstitial fluid

After the murine tumors were surgically removed and weighed, they were placed onto a 40 µM cell strainer that was inserted into a 50 mL tube. The cap was taped over the tube to hold the tumor and filter in place, and the tubes were centrifuged at 400×g for 5 minutes. The interstitial fluid collected at the bottom of the tubes was, if necessary, diluted with PBS. Mouse tumor interstitial fluid samples were analyzed using an R&D Systems Mouse Luminex Discovery Assay and a Luminex 200 (RRID: SCR_018025) Instrument (Luminex Corporation, LX200-XPON-RUO) according to the manufacturer's instructions. Quantitative analysis with 6 standards and a minimum of 50 counts per bead region was used with the Luminex assay to generate analyte values reported as picograms/milliliter (pg/mL). Samples beyond the lower and upper limits of detection were excluded from analysis. A Bicinchoninic acid assay was performed on all of the tumor intestinal fluid samples so that the analyte values from the cytokine analysis could be normalized to the total amount of protein in each sample, compensating for differential tumor size, fluid volume obtained, and dilution with PBS.

Immunohistochemistry

Mouse tumor tissue was fixed using 10% buffered formalin and subsequently paraffin-embedded. The tissue was cut into 5 µm sections with a microtome and mounted on glass slides for staining. This part of the procedure was completed by the Brown University

Molecular Pathology Core Facility. The slide wax solvent was removed using xylene, and then the slides were dehydrated with sequential immersion in decreasing concentrations of ethanol solution. The slides were boiled for 20 minutes using a Tris-EDTA buffer (pH 9.0) for antigen retrieval. The slides were then submerged in 3% hydrogen peroxide for 5 minutes to quench endogenous peroxidases. Then, horse serum (Vector Laboratories, #S-2012) was used to block non-specific binding for 30 minutes. The MOC1 and KPCY slides were then incubated in primary CD8 (Cell Signaling, #98941) or Ki-67 (Cell Signaling, #120202) antibody overnight at 4°C. The primary antibody was removed through TBST wash steps, and then the slides were incubated for 1 hour with a secondary antibody (Vector Laboratories, #MP-7401). The slides were then treated for 2 minutes with DAB substrate (Vector Laboratories, #SK-4100) to visualize the antibody staining. After a hematoxylin counterstain, the slides were again dehydrated with ethanol and finally mounted with coverslips and sealed. The entire slides were then scanned using an Olympus VS200 slide scanner (Olympus Lifesciences) at 10× magnification. The whole-slide scans were then quantified using the QuPath software (RRID: SCR_018257), where the percentage of CD8 or Ki67-positive cells was determined automatically.

RNA-seq analysis of patient treatment and outcome data

Kaplan-Meier curves were generated using TCGA RNA-seq data through the cBio portal, splitting the cohorts according to an *ITGB6* mRNA expression threshold of 0.25 standard deviations (σ) above and below the mean for the *ITGB6* high and *ITGB6* low cohorts, respectively. *ITGB6* expression and ICB response were evaluated with the Kaplan-Meier Plotter tool, and the *ITGB6* expression levels between ICB responders and non-responders were quantified using the ROC Plotter tool [16, 17]. The data was extracted using Python, and the figures were generated using GraphPad Prism (RRID: SCR_002798) version 10.

Statistical analysis

Statistical analysis and generation of figures were performed using GraphPad Prism. Graphed data show the dataset means and standard deviations. To compare statistical relationships between cohorts, two-tailed, paired T-tests or one-way ANOVA tests were performed where appropriate. Individual figure legends indicate the employment of statistical tests. Kaplan-Meier survival curves were generated using the Kaplan-Meier method and compared with Log-rank (Mantel-Cox) tests. Where *p*-values are not given directly, statistical significance is reported as $P < 0.05$: *, $P < 0.01$: **, $P < 0.001$: ***, and $P < 0.0001$: ****.

Results

ITGB6 is upregulated in cancer and is specific to malignant tissue

To determine the cancer types with sufficient magnitude and specificity of *ITGB6* expression to potentially make them suitable targets for inhibition, a TCGA analysis of *ITGB6* expression was performed (**Figure 1A**). Head and neck squamous cell carcinoma (HNSCC), pancreatic adenocarcinoma (PAAD), cervical cancer, lung adenocarcinoma, lung squamous cell carcinoma, as well as bladder cancer, all demonstrated high RNA expression of *ITGB6*.

The degree of specificity of *ITGB6* expression to cancerous tissue versus normal tissue can inform the efficacy of using blockade of *ITGB6* as a targeted therapy against cancer. For the cancer types identified as having high *ITGB6* expression, a comparison to their respective native tissues was drawn using RNA-seq data (**Figure 1B**). Head and neck squamous cell carcinoma (median fold-change (FC) 2.70, $P < 0.0001$), bladder urothelial carcinoma (FC 2.41, $P < 0.001$), pancreatic adenocarcinoma (FC 21.93, $P < 0.0001$), and cervical cancer (FC 2.03, $P < 0.0001$) showed upregulation of *ITGB6* compared to normal local tissue. Interestingly, lung adenocarcinoma (FC 0.77, $P < 0.04$) and lung squamous cell carcinoma (FC 0.55, $P < 0.0001$) showed downregulation of *ITGB6* compared to normal tissue.

Knockout of ITGB6 induces T-cell killing of HNSCC and PAAD cells

To identify a suitable *in vitro* model of *ITGB6*-expressing cancer, we preliminarily screened human cell lines based on their *ITGB6* RNA levels (**Figure 2A**). HNSCC cell lines FaDu and CAL27, as well as PAAD cell line Capan-2, were

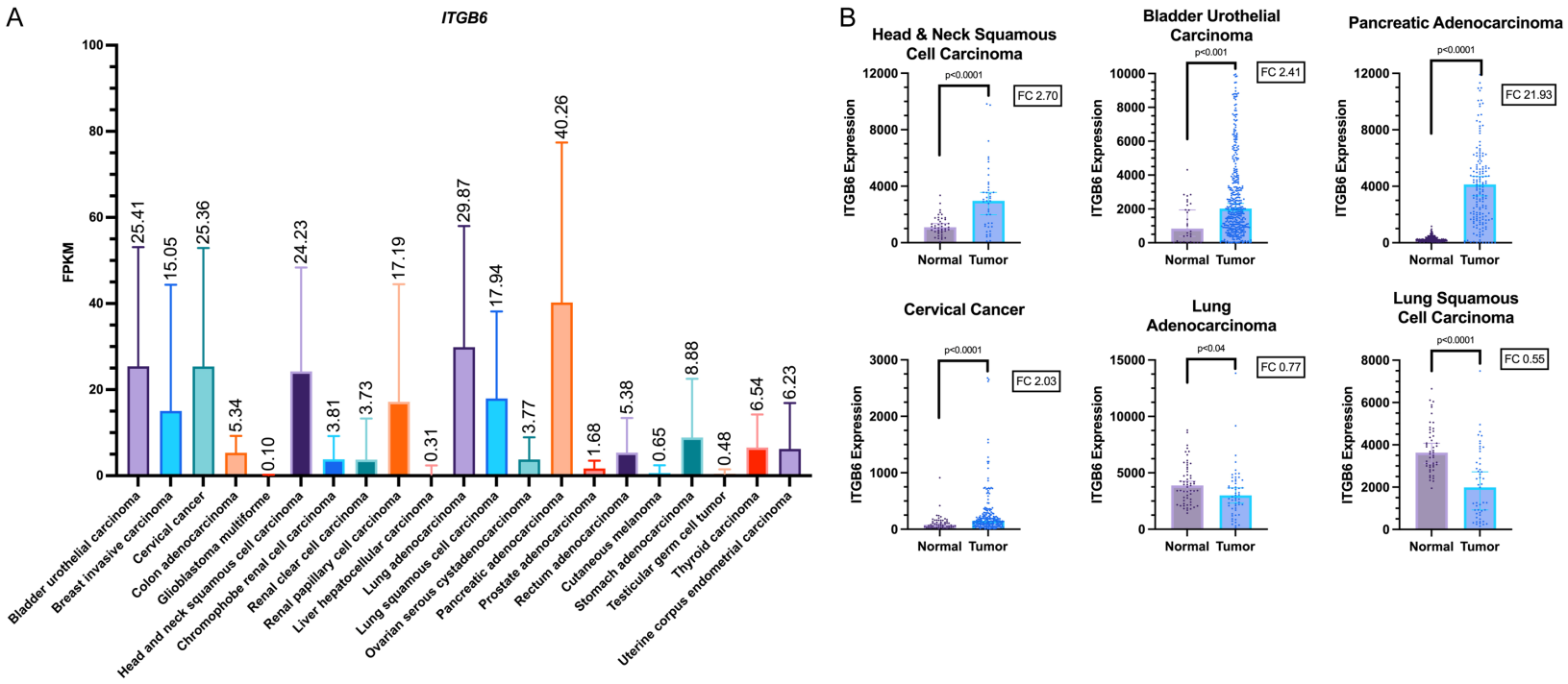

Figure 1. ITGB6 shows specificity and upregulation in human cancers. (A) Human Protein Atlas analysis of RNA expression of ITGB6 across various cancer types. Normalized RNA expression levels are given in fragments per kilobase million (FPKM). Data are acquired from TCGA. Graphs show the mean and SD. (B) Differential gene expression analysis of ITGB6 across tumor and normal tissue. Data are obtained from a standardized concatenated data set from GEO, GTex, TCGA, and TARGET databases. RNA-seq tumor and normal tissue samples are obtained from the same patients and from adjacent sites. Graphs were generated using the TNMplot tool and were normalized using DESeq2. Fold-change (FC) of medians and Mann-Whitney test *p*-values are shown.

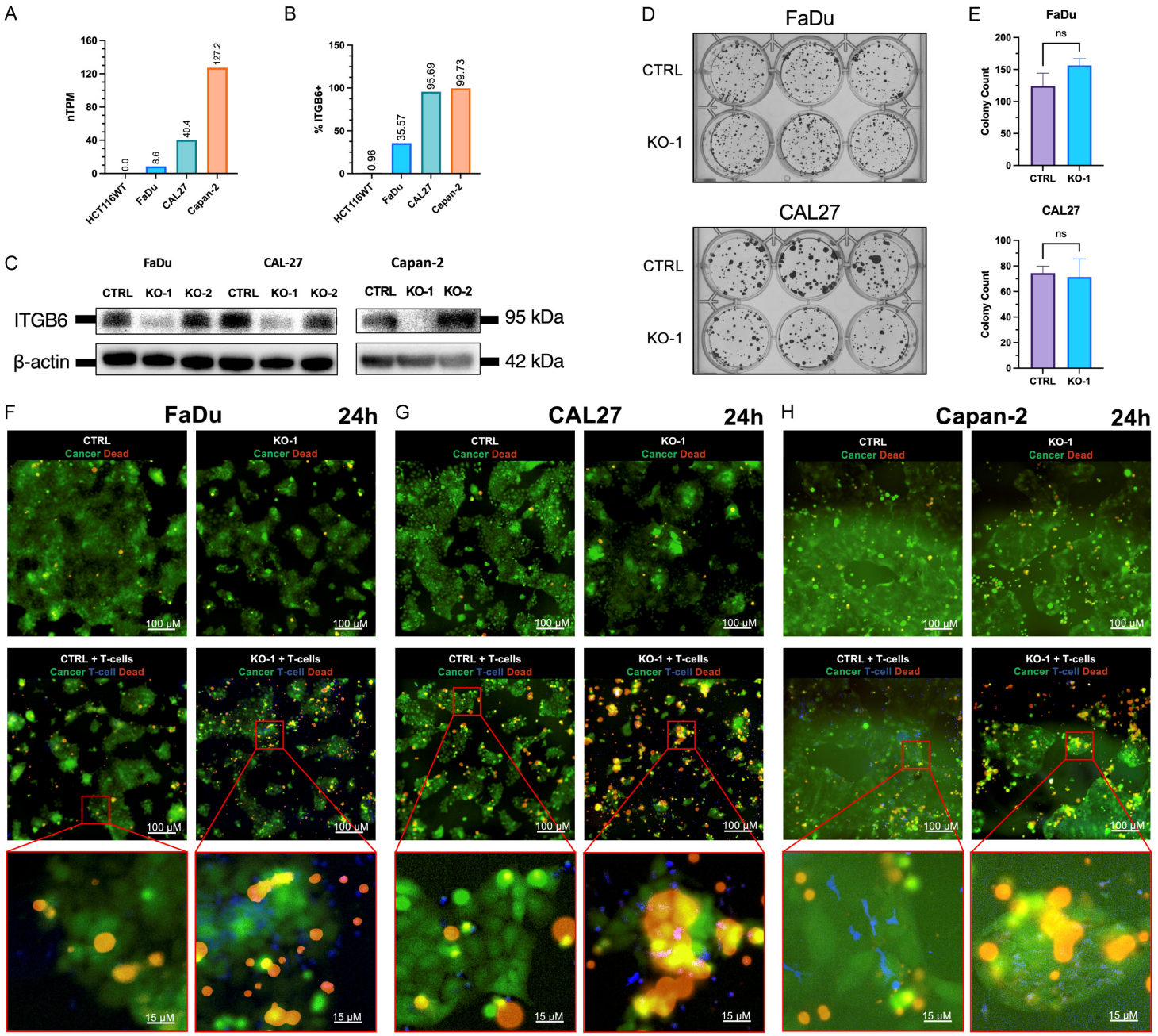
A
nTPM
160
120
80
40
0
0.0
8.6
40.4
127.2
HCT116WT
FaDu
CAL27
Capan-2
B
% ITGB6+
150
100
50
0
0.96
35.57
95.69
99.73
HCT116WT
FaDu
CAL27
Capan-2
C
FaDu
CAL-27
Capan-2
CTRL KO-1 KO-2 CTRL KO-1 KO-2 CTRL KO-1 KO-2
ITGB6
β-actin
95 kDa
42 kDa
D
FaDu
CTRL
KO-1
CAL27
CTRL
KO-1
E
FaDu
ns
Colony Count
200
150
100
50
0
CTRL
KO-1
CAL27
ns
Colony Count
100
80
60
40
20
0
CTRL
KO-1
F
FaDu
24h
G
CAL27
24h
H
Capan-2
24h
CTRL
Cancer Dead
KO-1
Cancer Dead
CTRL + T-cells
Cancer T-cell Dead
KO-1 + T-cells
Cancer T-cell Dead
100 μM
15 μM

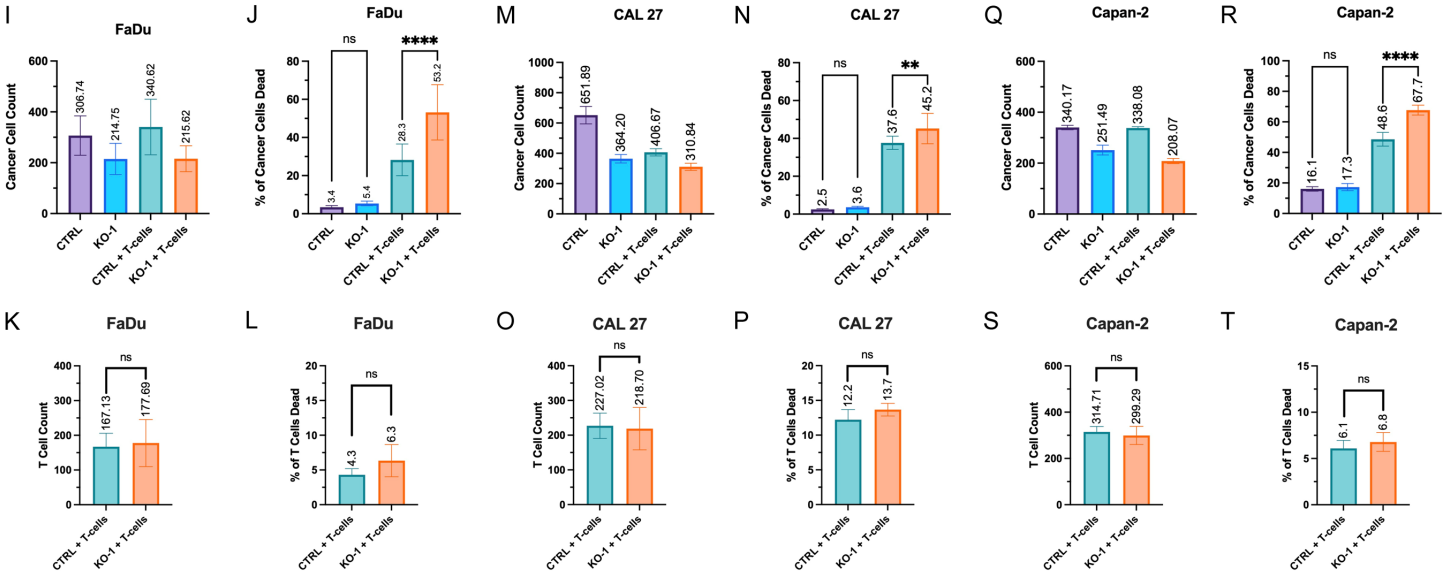

Figure 2. *ITGB6* knockout induces T-cell killing of HNSCC and PAAD cells. (A) ITGB6 RNA of selected human cancer cell lines from the Human Protein Atlas. (B) Flow cytometry analysis of the percentage of cancer cells that are ITGB6+ compared to unstained controls. (C) Western blot validation of the CRISPR knockout of ITGB6 in FaDu, CAL27, and Capan-2 cells. (D) Colony formation assay of CRISPR control (CTRL) cells and ITGB6 knockouts (KO-1) for FaDu and CAL27 cells (n = 3). (E) Quantification of colony formation assay. Statistical analysis was performed using an unpaired t-test. Randomly chosen fields of view from the co-culture of FaDu (F), CAL-27 (G), or Capan-2 (H) cells (green) and TALL-104 T-cells (blue) (n = 10). Cells were pretreated for 8 hrs with latent TGFβ. Quantification of cancer cell counts for FaDu (I), CAL27 (M), and Capan-2 (Q). Quantification of the percentage of cancer cells that are dead for FaDu (J), CAL27 (N), and Capan-2 (R). Quantification of TALL-104 T-cell counts for the FaDu cohort (K), the CAL27 cohort (O), and the Capan-2 cohort (S). Quantification of the percentage of T cells that are dead for the FaDu cohort (L), the CAL27 cohort (P), and the Capan-2 cohort (T). One-way ANOVA: $P < 0.0001$ (****), $P < 0.01$ (**).

subjected to flow cytometric analysis of ITGB6 expression (**Figure 2B**). With the colon carcinoma cell line HCT116WT serving as a negative control (0.96% ITGB6+), FaDu cells showed moderate ITGB6 expression (35.57%), while CAL27 and Capan-2 cells showed high ITGB6 expression (95.69% and 99.73% respectively).

Furthermore, cell lines FaDu, CAL27, and Capan-2 were transfected with Cas9 protein to induce a CRISPR knockout of *ITGB6* in the cells. A western blot validation of the treated cells revealed a high-efficiency knockout of *ITGB6* in the cells using guide RNA-1 (KO-1) and RNA-2 (KO-2) (**Figure 2C**).

To facilitate a study of the immune implications of *ITGB6,* we sought to validate that the knockout cells we created did not exhibit significantly altered intrinsic growth behavior. To this end, a 10-day colony formation assay was performed, which revealed no significant change in cell survival and colony formation potential between control and *ITGB6* knockout cells in the two models of HNSCC (**Figure 2D**, **2E**). The absence of a differential tumor colony formation rate over 10 days further suggests that the increased cancer cell death seen over the relatively short 24-hour co-culture experiments described below may be primarily immune-mediated.

The knockout cells with guide RNA-1 (KO-1), as well as the non-targeting control guide cells (CTRL), were co-cultured with TALL-104 T-cells to study the immunoprotective effect of *ITGB6* in HNSCC and PAAD cells (**Figure 2F-H**). The co-cultures were treated with 10 ng/ml of latent TGFβ for 8 hours to simulate sequestered TGFβ present in the tumor microenvironment. The experiment was conducted with 10 replicates per condition. Quantitative fluorescence microscopy of the co-culture revealed that the knockout of *ITGB6* substantially increased T-cell killing over 24 hours in FaDu cells (FaDu CTRL 28.26% ± 8.29 dead vs. FaDu KO-1 53.18% ± 14.50 dead, $P < 0.0001$), CAL27 cells (CAL27 CTRL 37.64% ± 3.51 dead vs. CAL27 KO-1 45.21% ± 8.02 dead, $P < 0.01$), and Capan-2 cells (Capan-2 CTRL 48.62% ± 4.26 dead vs. Capan-2 KO-1 67.73% ± 3.07 dead, $P < 0.0001$) (**Figure 2J**, **2N**, **2R**). In the conditions without T-cells, the number of *ITGB6* knockout cancer cells across all three cell lines was reduced relative to CTRL cells, indicating that the loss of *ITGB6* may nonetheless alter the intrinsic characteristics of cancer cells (**Figure 2I**, **2M**, **2Q**). To account for any intrinsic effects and to measure only T-cell mediated killing of cancer cells, the percentage of dead cancer cells was determined by counting only events of colocalization of the cell death dye (yellow) onto the fluorescent channel of the cancer cells (green) (**Figure 2J**, **2N**, **2R**). This method allows for the quantification of cancer cell death mediated by cytotoxic T-cells while accounting for any potential *ITGB6* status-dependent differences in cancer cell growth characteristics. Furthermore, the knockout condition visually exhibited a higher density of T-cells in the proximity of cancer cells as compared to the control condition (**Figure 2F-H**). The quantities of T-cells (**Figure 2K**, **2O**, **2S**), as well as the percentage of T-cells exhibiting cell death stain (**Figure 2L**, **2P**, **2T**) were also measured, demonstrating that T-cell death was minimal overall and did not differ across *ITGB6* status. The increased T-cell killing of cancer cells upon *ITGB6* inhibition was also validated using a doxycycline-inducible shRNA knockdown system in FaDu cells (Figure S1).

Tumor ITGB6 knockout reduces tumor progression in immunocompetent mice

To demonstrate the anti-tumor activity of *ITGB6* knockout *in vivo*, suitable HNSCC and PAAD cell lines were identified for heterotopic injection into immunocompetent mice. Identification of cell lines with high ITGB6 expression was performed via flow cytometry. The CT26 colon carcinoma cell line, known to have low ITGB6 expression, was used as a negative control (1.96% ITGB6+) [3] (**Figure 3A**). The HNSCC cell line MOC2 showed moderate ITGB6 expression (28.36% ITGB6+) while MOC1 and the PAAD cell line KPCY showed high expression (82.97% and 53.07% respectively). As with the human cell lines, MOC1 cells and KPCY were selected for *ITGB6* knockout using CRISPR, which was validated via western blot (**Figure 3B**).

To validate that any change in *in vivo* growth rate is not primarily attributed to differences in intrinsic tumor growth characteristics between *ITGB6* knockout and control cells, again, colony formation assays were performed (**Figure 3C**, **3D**). After 10 days, MOC1 cells showed a slightly decreased colony formation rate across both *ITGB6* knockout guide RNAs, with knockout cell line KO-2 reaching statistical significance ($P <$

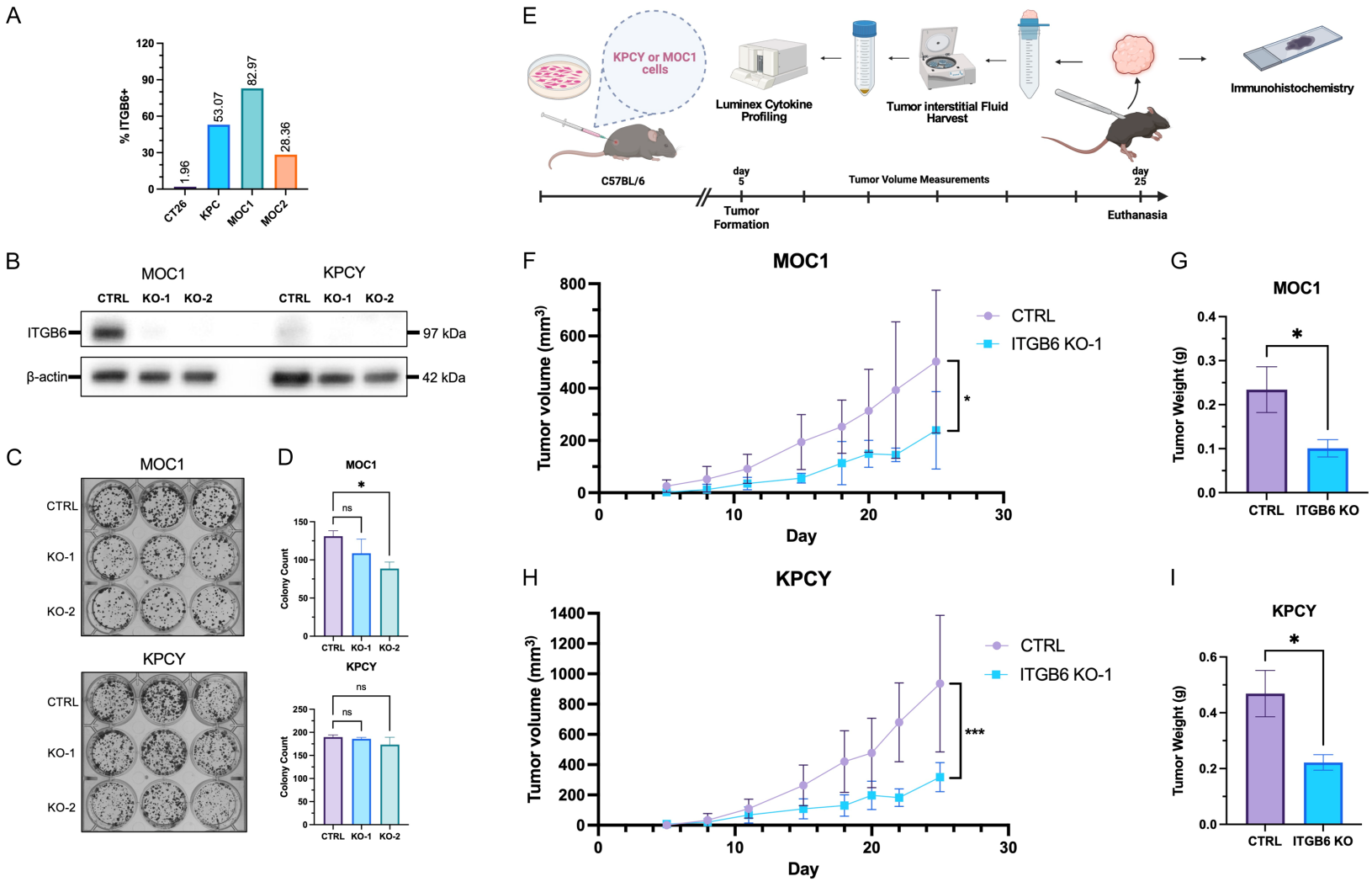
A
% ITGB6+
120
90
60
30
0
1.96
53.07
82.97
28.36
CT26
KPC
MOC1
MOC2
B
MOC1
KPCY
CTRL
KO-1
KO-2
CTRL
KO-1
KO-2
ITGB6
β-actin
97 kDa
42 kDa
C
MOC1
CTRL
KO-1
KO-2
KPCY
CTRL
KO-1
KO-2
D
MOC1
*
ns
Colony Count
150
100
50
0
CTRL
KO-1
KO-2
KPCY
ns
ns
Colony Count
250
200
150
100
50
0
CTRL
KO-1
KO-2
E
KPCY or MOC1 cells
Luminex Cytokine Profiling
Tumor interstitial Fluid Harvest
Immunohistochemistry
C57BL/6
day 5
Tumor Formation
Tumor Volume Measurements
day 25
Euthanasia
F
MOC1
Tumor volume (mm3)
800
600
400
200
0
0
10
20
30
Day
CTRL
ITGB6 KO-1
*
G
MOC1
Tumor Weight (g)
0.4
0.3
0.2
0.1
0.0
*
CTRL
ITGB6 KO
H
KPCY
Tumor volume (mm3)
1400
1200
1000
800
600
400
200
0
0
10
20
30
Day
CTRL
ITGB6 KO-1
***
I
KPCY
Tumor Weight (g)
0.6
0.4
0.2
0.0
*
CTRL
ITGB6 KO

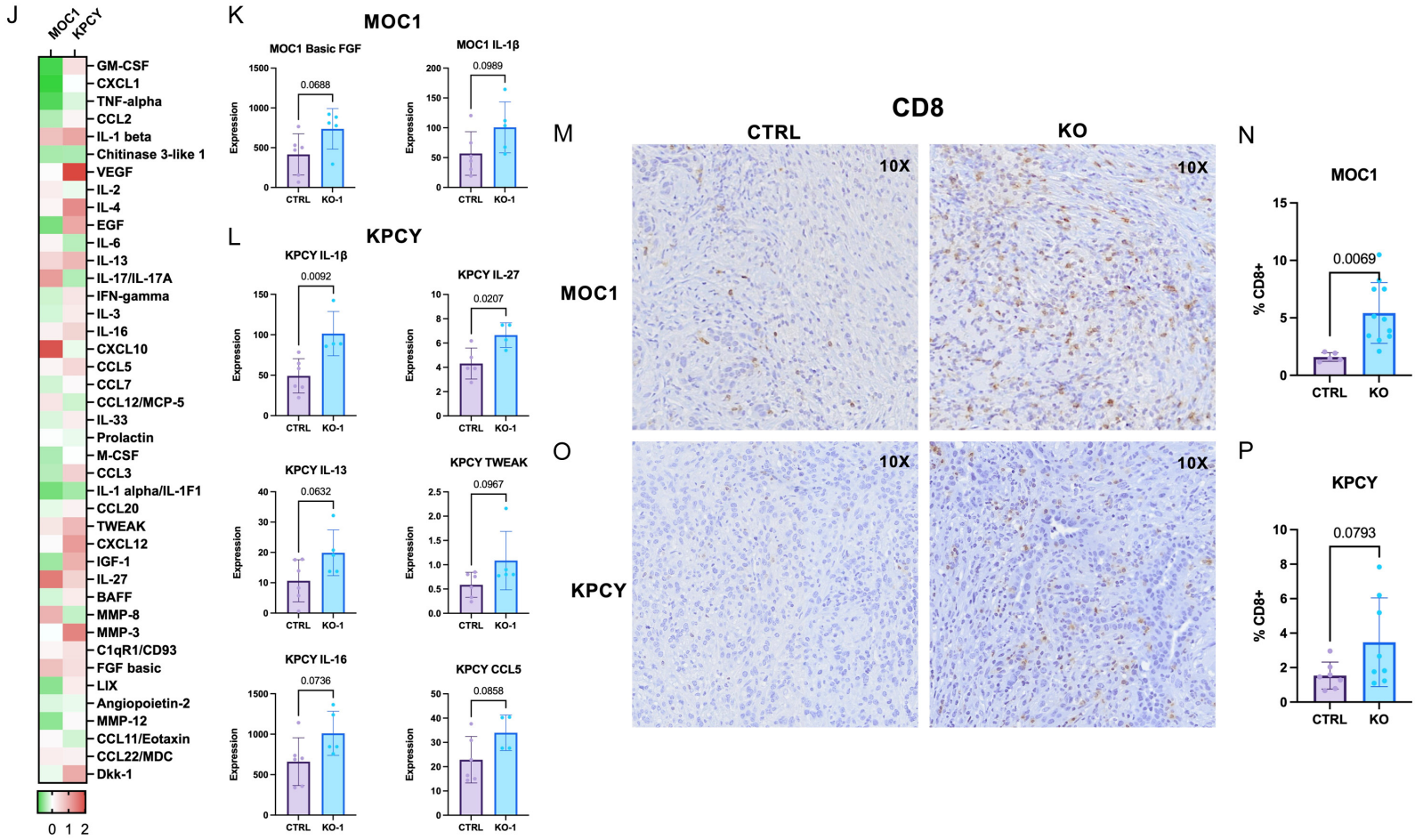

Figure 3. Suppressed growth of *ITGB6*-knockout tumors in immunocompetent mice. (A) Flow cytometry analysis of the percentage of mouse cancer cells that are ITGB6+ compared to unstained controls. (B) Western blot validation of CRISPR knockdown of ITGB6 in MOC1 and KPCY cells. (C) Colony formation assay of CRISPR control (CTRL) cells and ITGB6-knockout (KO-1, KO-2) cells for MOC1 and KPCY cells. (D) Quantification of colony formation assay. Statistical analysis was performed using one-way ANOVA: $P < 0.05$ (*). (E) Experimental timeline for C57BL/6 mice injected with syngeneic tumor cells. Tumor volume of mice starting upon tumor formation at day 5 for MOC1 (F) and KPCY (H) cohorts (n = 10). Mass of MOC1 (G) and KPCY (I) tumors harvested at day 25. Statistical comparison between CTRL and KO-1 cohorts was performed using an unpaired t-test: $P < 0.001$ (***), $P < 0.05$ (*). (J) Heat map of Luminex panel showing fold change of cytokines of tumor interstitial fluid harvested from MOC1 and KPCY tumors (n = 5). Red indicates upregulation and green downregulation of cytokines in ITGB6 KO tumors compared to control tumors. (K) Concentrations of select tumor interstitial fluid cytokines from MOC1 and KPCY (L) as measured by the Luminex panel. Statistical comparison between CTRL and KO-1 cohorts was performed using an unpaired t-test. Representative 10× images of MOC1 (M) and KPCY (O) from scanned IHC slides showing CD8 T-cell infiltration across control and ITGB6-deficient cells. Quantification of CD8-stained IHC slides for MOC1 (N) (control: n = 5, KO: n = 10) and KPCY (P) (control: n = 7, KO: n = 8) cohorts, showing *p*-values calculated using an unpaired t-test.

0.05). KPCY cells showed no observable difference in colony formation rate.

MOC1 and KPCY cohorts of C57BL/6 mice received flank injections of either CTRL or KO-1 cells (**Figure 3E**). Each of the four groups contained 10 mice with an equal male-to-female ratio. The *ITGB6* knockout cells demonstrated reduced tumor progression compared to control cells over the 25-day course of the experiment. At day 25, both MOC1 (MOC1 CTRL 502.46 mm^3 ± 273.45 mm^3 vs. MOC1 KO-1 239.03 mm^3 ± 147.85 mm^3, P = 0.0217) and KPCY (KPCY CTRL 935.83 mm^3 ± 451.08 mm^3 vs. KPCY KO-1 317.76 mm^3 ± 95.80 mm^3, P = 0.0002) cohorts showed significantly reduced tumor volumes for the *ITGB6* deficient tumors (**Figure 3F**, **3H**). Additionally, there was a substantial difference in the mass of the excised tumors at the end of the experiment for both MOC1 (MOC1 CTRL 0.234 g ± 0.147 g vs. MOC1 KO-1 0.101 g ± 0.059 g, P = 0.0239) and KPCY (KPCY CTRL 0.469 g ± 0.287 g vs. KPCY KO-1 0.222 g ± 0.092 g, P = 0.0128) cohorts (**Figure 3G**, **3I**). Mice across all cohorts demonstrated no meaningful change in body mass (Figure S2). Additionally, to confirm that knockout of *ITGB6* did not alter the intrinsic proliferation rate of MOC1 and KPCY cells in vivo, immunohistochemistry of paraffin-embedded tissue slides for Ki-67 staining was completed, with no statistically significant changes across the control and knockout cells (Figure S3).

Knockout of ITGB6 increases CD8 T-cell infiltration and TME anti-tumor cytokines

Immunohistochemistry revealed markedly increased CD8 T-cell infiltration upon *ITGB6* inhibition in harvested MOC1 and KPCY tumors, with representative images shown (**Figure 3M**, **3O**). Quantification of entire tumor cross-sections through high-resolution scanning of tissue slides revealed a potent and statically significant increase in CD8 T-cell infiltration in *ITGB6* inhibited MOC1 tumors (MOC1 CTRL 1.599% ± 0.334 vs. MOC1 KO-1 5.753% ± 2.402, P = 0.0033) and to a lesser degree in KPCY (KPCY CTRL 1.539% ± 0.726 vs. KPCY KO-1 3.473% ± 2.409, P = 0.0793) tumors (**Figure 3N**, **3P**). It must be noted that the KPC(Y) cell line is a murine PAAD model that authentically recapitulates the lack of T-cells observed clinically in PAAD [18, 19]. Therefore, the more than doubling of CD8 positive cells in the *ITGB6* knockout KPCY cohort may represent a therapeutically meaningful change in the TME that is conceivably driving the drastically reduced *in vivo* tumor growth.

To further evaluate changes in the TME, the tumor interstitial fluid from the harvested lesions was collected via centrifugation to be analyzed via a multiplexed cytokine discovery panel. Fold changes for the cytokines GM-CSF, CXCL1, TNF-alpha, CCL2, IL-1β, Chitinase 3, VEGF, IL-2, IL-4, EGF, IL-6, IL-13, IL17, IFN-γ, IL-3, IL-16, CXCL10, CCL5, CCL7, CCL12, IL-33, Prolactin, M-CSF, CCL3, IL-1α, CCL20, TWEAK, CXCL12, IGF-1, IL-27, BAFF, MMP-8, MMP-3, C1qR1, FGF basic, LIX, Angiopoietin-2, MMP-12, CCL11, CCL22, and Dkk-1 are shown (**Figure 3J**). Additionally, select cytokines with the lowest *p*-values are graphed individually (**Figure 3K**, **3L**). This analysis revealed upregulation of cytokines associated with T-cell antitumor activity and other signals of immune activation in the *ITGB6* knockout cohorts. Both MOC1 and KPCY tumors with *ITGB6* deficiency showed upregulation of IL-1β, a marker of immune cell activation that is associated with greater cytotoxicity of CD8 T-cells and has been previously shown to correlate with T-cell-mediated regression of mouse model tumors [20]. Additionally, KPCY *ITGB6* knockout tumors exhibited increased IL-27, a sign of CD8, CD4, and potentially NK cell activation [21]. IL-27 has been shown to mediate a potent T-cell antitumor response [22]. There was also an increase in IL-13, IL-16, Tweak, and CCL5 in KPCY tumors, as well as an increase in FGFbasic in MOC1 tumors.

High ITGB6 leads to decreased patient survival in squamous cell cancers and pancreatic adenocarcinoma

To investigate how the *in vitro* and *in vivo* results compare to the clinic, an analysis of patient survival using TCGA patient outcome data was performed. TCGA RNA-seq data revealed that high *ITGB6* expression was a potent marker of a poor prognosis in head and neck squamous cell carcinoma (high *ITGB6* median survival 35.51 mos. vs. low *ITGB6* 57.88 mos., P = 0.0090), pancreatic adenocarcinoma (high *ITGB6* median survival 15.64 mos. vs. low *ITGB6* 22.70 mos., P = 0.0002), lung squamous cell carcinoma (high *ITGB6* median survival 61.56 mos. vs. low *ITGB6*

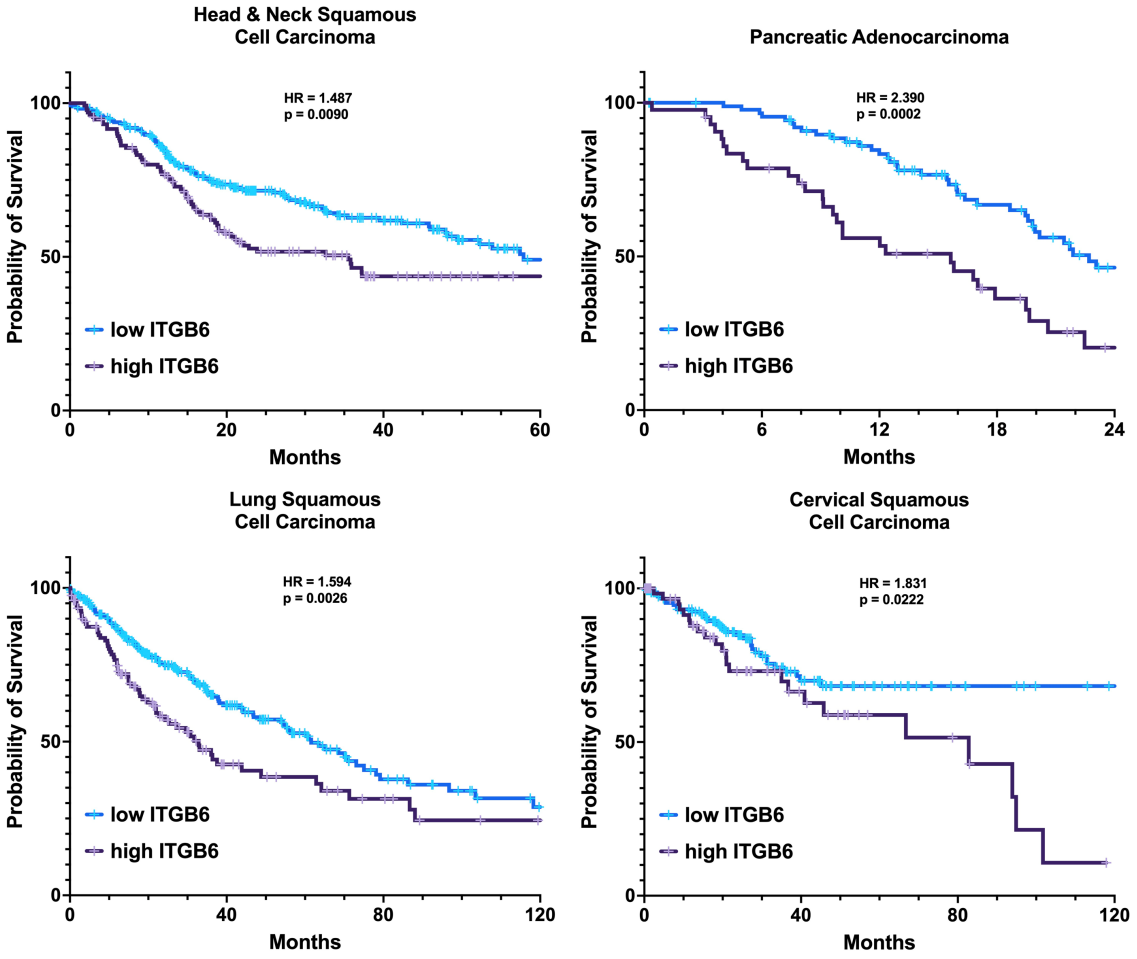

Figure 4. ITGB6 decreases overall survival in patients. Curves show the overall survival of patients with various cancer types stratified based on ITGB6 expression. Patients with high ITGB6 have expression levels above +0.25 σ of the mean, and ITGB6 low patients have expression below -0.25 σ. The graphs were generated using TCGA data through the cBioPortal. Statistical analysis of Kaplan-Meier curves and corresponding hazard ratios (HR) was performed using the Log-rank test.

32.85 mos., P = 0.0026), and cervical squamous cell carcinoma (high *ITGB6* median survival is undefined, low *ITGB6* 82.79 mos., P = 0.0222) (**Figure 4**). Statistical analysis was performed using the Log-rank (Mantel-Cox) test.

High ITGB6 expression impairs response to αPD-1 and αPD-L1 immune checkpoint blockade and enhances CTLA-4 response

In a pan-cancer analysis of patients receiving α-PD-1 or α-PD-L1 immune checkpoint blockade, ICB non-responders had higher *ITGB6* expression. Non-responders to α-PD-1 therapy had an *ITGB6* expression fold change of 1.794 (P = 0.046) while α-PD-L1 non-responders had an *ITGB6* fold change of 1.336 (P = 0.023) compared to responders (**Figure 5A**). For patients receiving CTLA-4 therapy, this relationship was reversed, with non-responders having an *ITGB6* expression fold change of 0.670 (P = 0.622); however, this relationship did not reach statistical significance.

Furthermore, patient outcome data revealed that high *ITGB6* expression was a marker of a poor prognosis in patients receiving α-PD-1 therapy (high *ITGB6* 19.94 mos. vs. low *ITGB6* 23.59 mos., P = 0.0407) and patients receiving α-PD-L1 therapy (high *ITGB6* 8.77 mos. vs. low *ITGB6* 17.08 mos., P = 0.0012) (**Figure 5B**). However, patients receiving α-CTLA-4 therapy had better outcomes with high *ITGB6* expression (high *ITGB6* 28.43 mos. vs. low *ITGB6*

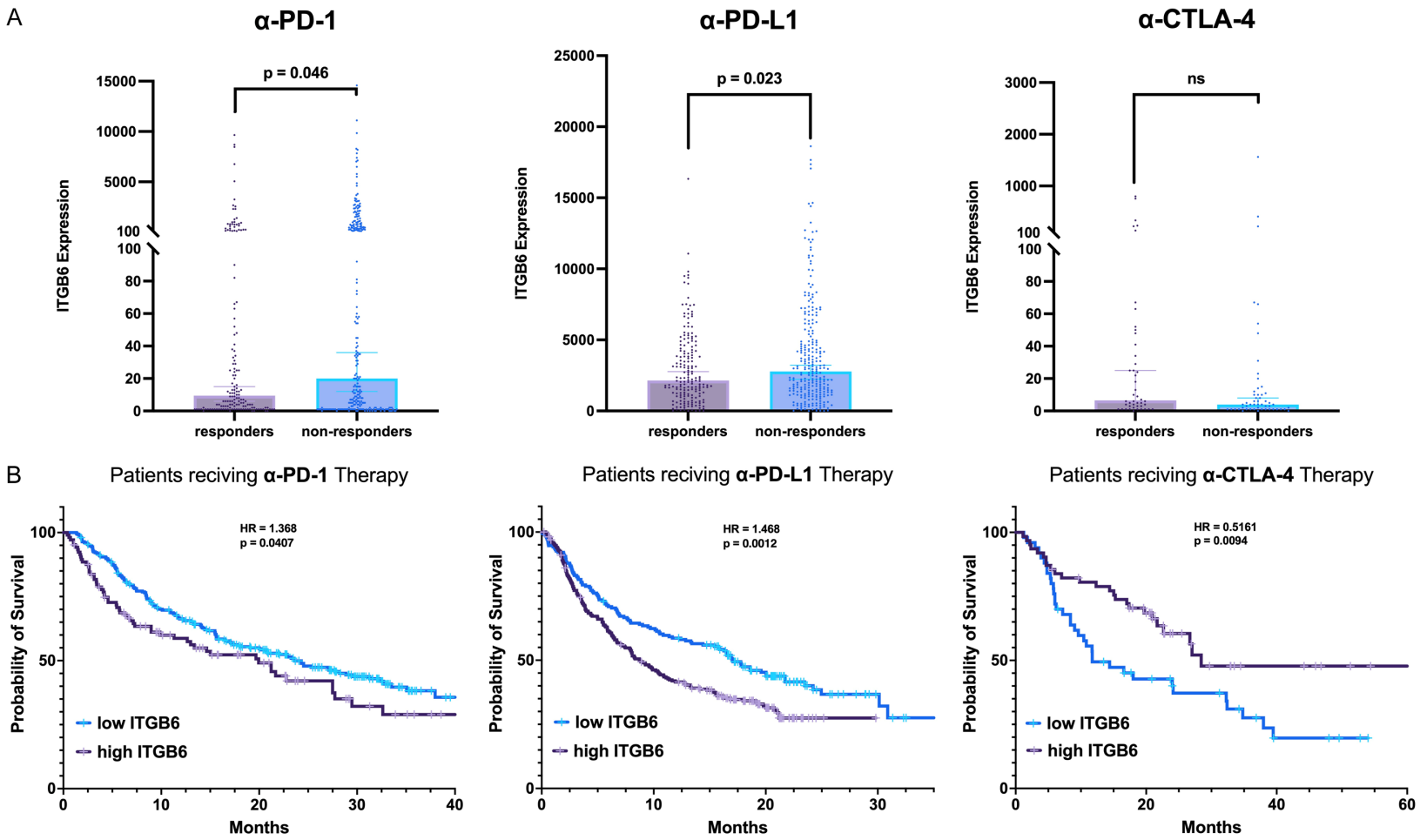

Figure 5. Immune checkpoint blockade is modulated by ITGB6 expression. (A) Pan-cancer analysis of ITGB6 RNA expression level normalized using DESeq2 of patients who are either responsive or unresponsive to immune checkpoint blockade. RNA data are extracted from a TCGA data set of multiple cancer types of patients who underwent immune checkpoint blockade therapy. Graphs were generated using the ROCplot tool, and the results of an unpaired t-test are shown. (B) Kaplan-Meier curves of overall survival of patients undergoing immune checkpoint blockade therapy stratified into low and high ITGB6 expression about the mean. Statistical analysis was performed using the Log-rank test.

11.73 mos., P = 0.0094). Statistical analysis was performed using the Log-rank (Mantel-Cox) test.

Discussion

The integrin αvβ6 and its β subunit ITGB6 are promising targets for several solid tumors. Squamous cell carcinomas of the head and neck, cervix, and lung, as well as pancreatic adenocarcinomas, commonly have upregulated ITGB6 (**Figure 1A**). Our *in vivo* experiments with mouse models of head and neck squamous cell carcinoma (HNSCC) and pancreatic adenocarcinoma (PAAD) showed potent antitumor activity in models of two of the most detrimental cancer types globally (**Figure 3**) [23]. The strong reduction of cancer growth and increased CD8 T-cell infiltration observed in our mouse experiments demonstrates that ITGB6 is a target that could be used to potentiate an anti-tumor T-cell response in human HNSCC and PAAD (**Figure 3M-P**). Upregulation of IL-1β and IL-27 further suggests that ITGB6 inhibition increases the efficacy and anti-tumor activity of T-cells in the TME (**Figure 3J-L**) [20, 21]. Short-term experiments with *ITGB6* knockout cancer cells, co-cultured with T-cells, plausibly indicate that the success observed in our animal models is through the regulation of T-cells (**Figure 2**). However, future experiments using functional blockade of T-cells or TGFβ will serve to more clearly define this mechanism. Nonetheless, the absence of a substantial growth disadvantage due to ITGB6 knockout in our colony formation assays provides further evidence for an immune-mediated mechanism (**Figure 2D**, **2E**).

Our analysis of clinical data shows that our *in vitro* and *in vivo* experiments recapitulate the role of *ITGB6* in the clinic. *ITGB6* upregulation is associated with worse outcomes in cancer patients, especially in HNSCC and PAAD, but also in lung squamous cell carcinoma and cervical squamous cell carcinoma (**Figure 4**). Fortunately, the high specificity of ITGB6 to tumor tissue presents as a promising therapeutic opportunity for targeting cancer cells locally while sparing surrounding tissues and minimizing systemic toxicity (**Figure 1B**). Promising results with antibody-drug conjugate (ADC) sigvotatug vedotin in NSCLC, which uses ITGB6 to hone an antineoplastic payload to cancer cells, provide encouragement for ITGB6 as a therapeutic target [24, 25]. However, sigvotatug vedotin, designed as an ADC, does not block ITGB6 at therapeutically meaningful doses [24]. Our results from genetic inhibition of *ITGB6* in mouse tumors and analysis of clinical data suggest that functional blockade of ITGB6 could provide therapeutic value beyond using ITGB6 solely as a target antigen.

Lastly, we have also observed that *ITGB6* expression in patients can lead to inferior responses to common immune checkpoint blockade therapies (**Figure 5A**, **5B**). The patient outcome data correlating low *ITGB6* expression to positive immune checkpoint blockade response offer encouragement to investigate treatment combinations of ITGB6 blockade with clinically relevant immune checkpoint inhibitors. While high *ITGB6* expression interfered with anti-PD-1/PD-L1 response, it was surprising to find that patients receiving anti-CTLA-4 therapy had a worse prognosis when *ITGB6* expression was low, an observation that should be investigated further. Additionally, it is surprising that high *ITGB6* is also a predictor of poor prognosis in lung squamous cell carcinoma, although levels of *ITGB6* appear to be higher in non-cancerous lung tissue compared to squamous cell carcinoma. This observation suggests, not unexpectedly, that aberrant *ITGB6* exists in the context of other oncogenic alterations necessary to harness the immune evasive effects of *ITGB6*. Future studies will hopefully be able to uncover the intricacies of these mechanisms. Nevertheless, our data tentatively suggest that ITGB6 blockade could perhaps sensitize patients to ICB who would otherwise see no benefit from the therapy. Combination therapies of ITGB6 blockade with immune checkpoint inhibitors such as α-PD-1, α-41-BB, and α-LAG-3 will be of particular interest to our group. Results from functional αvβ6 blockade in colorectal cancer have convincingly demonstrated a mechanism that attributes the therapeutic effect of αvβ6 blockade to tumor TGFβ paracrine disruption of T-cells in a mouse model with TGFβ receptor-deficient T-cells [3]. A reliable assay to assess the dynamics of TGFβ *in vitro* and *in vivo*, through reporter cell lines or antibody-based techniques, has remained elusive and was not incorporated in the present study. However, such experiments are planned by our group in the future to perform a more comprehensive characterization of the immune mechanisms involved in HNSCC and PAAD with respect to *ITGB6* and TGFβ. Nonetheless, the

efficacy of the therapeutic immune response we observed following *ITGB6* inhibition provides a convincing rationale for the therapeutic development of anti-ITGB6 compounds. Future studies will serve to translate the pharmacological or biological targeting of ITGB6 into therapeutic clinical trials.

Acknowledgements

W.S.E-D. is an American Cancer Society Research Professor and is supported by the Mencoff Family University Professorship at Brown University.

Disclosure of conflict of interest

None.

Address correspondence to: Wafik S El-Deiry, Laboratory of Translational Oncology and Experimental Cancer Therapeutics, The Warren Alpert Medical School, Brown University, Providence, RI 02903, USA. E-mail: wafik@brown.edu

References

[1] Chen S, Zhang Z, Zheng X, Tao H, Zhang S, Ma J, Liu Z, Wang J, Qian Y, Cui P, Huang D, Huang Z, Wu Z and Hu Y. Response efficacy of PD-1 and PD-L1 inhibitors in clinical trials: a systematic review and meta-analysis. Front Oncol 2021; 11: 562315.

[2] Zhang Q, Zhang S, Chen J and Xie Z. The interplay between integrins and immune cells as a regulator in cancer immunology. Int J Mol Sci 2023; 24: 6710.

[3] Busenhart P, Montalban-Arques A, Katkeviciute E, Morsy Y, Van Passen C, Hering L, Atrott K, Lang S, Garzon JFG, Naschberger E, Hartmann A, Rogler G, Stürzl M, Spalinger MR and Scharl M. Inhibition of integrin αvβ6 sparks T-cell antitumor response and enhances immune checkpoint blockade therapy in colorectal cancer. J Immunother Cancer 2022; 10: e003465.

[4] Meecham A and Marshall JF. The ITGB6 gene: its role in experimental and clinical biology. Gene X 2020; 5: 100023.

[5] Massagué J. TGFbeta in Cancer. Cell 2008; 134: 215-230.

[6] Horiguchi M, Ota M and Rifkin DB. Matrix control of transforming growth factor-β function. J Biochem 2012; 152: 321-329.

[7] Sanjabi S, Oh SA and Li MO. Regulation of the immune response by TGF-β: from conception to autoimmunity and infection. Cold Spring Harb Perspect Biol 2017; 9: a022236.

[8] Ortiz-Muñoz G, Brown M, Carbone CB, Pechuan-Jorge X, Rouilly V, Lindberg H, Ritter AT, Raghupathi G, Sun Q, Nicotra T, Mantri SR, Yang A, Doerr J, Nagarkar D, Darmanis S, Haley B, Mariathasan S, Wang Y, Gomez-Roca C, de Andrea CE, Spigel D, Wu T, Delamarre L, Schöneberg J, Modrusan Z, Price R, Turley SJ, Mellman I and Moussion C. In situ tumour arrays reveal early environmental control of cancer immunity. Nature 2023; 618: 827-833.

[9] Katsuno Y, Meyer DS, Zhang Z, Shokat KM, Akhurst RJ, Miyazono K and Derynck R. Chronic TGF-β exposure drives stabilized EMT, tumor stemness, and cancer drug resistance with vulnerability to bitopic mTOR inhibition. Sci Signal 2019; 12: eaau8544.

[10] MacDonald WJ, Srinivasan PR, Pinho-Schwermann M, Tajiknia V, Purcell C, Carlsen L and El-Deiry WS. Abstract 5140: ITGB6 as a predictive biomarker for overall prognosis and PD-(L)1 immune checkpoint blockade response in various cancer types. Cancer Research 2024; 84: 5140.

[11] Liu S, Wang J, Niu W, Liu E, Wang J, Peng C, Lin P, Wang B, Khan AQ, Gao H, Liang B, Shahbaz M and Niu J. The β6-integrin-ERK/MAP kinase pathway contributes to chemo resistance in colon cancer. Cancer Lett 2013; 328: 325-334.

[12] You B, Pan S, Gu M, Zhang K, Xia T, Zhang S, Chen W, Xie H, Fan Y, Yao H, Cheng T, Zhang P, Liu D and You Y. Extracellular vesicles rich in HAX1 promote angiogenesis by modulating ITGB6 translation. J Extracell Vesicles 2022; 11: e12221.

[13] Zhang C, Li K, Zhu H, Cheng M, Chen S, Ling R, Wang C and Chen D. ITGB6 modulates resistance to anti-CD276 therapy in head and neck cancer by promoting PF4+ macrophage infiltration. Nat Commun 2024; 15: 7077.

[14] Love MI, Huber W and Anders S. Moderated estimation of fold change and dispersion for RNA-seq data with DESeq2. Genome Biol 2014; 15: 550.

[15] Bartha Á and Győrffy B. TNMplot.com: a web tool for the comparison of gene expression in normal, tumor and metastatic tissues. Int J Mol Sci 2021; 22: 2622.

[16] Fekete JT and Győrffy B. ROCplot.org: Validating predictive biomarkers of chemotherapy/hormonal therapy/anti-HER2 therapy using transcriptomic data of 3,104 breast cancer patients. Int J Cancer 2019; 145: 3140-3151.

[17] Győrffy B. Survival analysis across the entire transcriptome identifies biomarkers with the highest prognostic power in breast cancer. Comput Struct Biotechnol J 2021; 19: 4101-4109.

[18] Goulart MR, Stasinos K, Fincham REA, Delvecchio FR and Kocher HM. T cells in pancreatic cancer stroma. World J Gastroenterol 2021; 27: 7956-7968.
[19] Pham TND, Shields MA, Spaulding C, Principe DR, Li B, Underwood PW, Trevino JG, Bentrem DJ and Munshi HG. Preclinical models of pancreatic ductal adenocarcinoma and their utility in immunotherapy studies. Cancers (Basel) 2021; 13: 440.
[20] Shi J, Song X, Traub B, Luxenhofer M and Kornmann M. Involvement of IL-4, IL-13 and their receptors in pancreatic cancer. Int J Mol Sci 2021; 22: 2998.
[21] Kourko O, Seaver K, Odoardi N, Basta S and Gee K. IL-27, IL-30, and IL-35: a cytokine triumvirate in cancer. Front Oncol 2019; 9: 969.
[22] Ben-Sasson SZ, Hogg A, Hu-Li J, Wingfield P, Chen X, Crank M, Caucheteux S, Ratner-Hurevich M, Berzofsky JA, Nir-Paz R and Paul WE. IL-1 enhances expansion, effector function, tissue localization, and memory response of antigen-specific CD8 T cells. J Exp Med 2013; 210: 491-502.
[23] Mattiuzzi C and Lippi G. Current cancer epidemiology. J Epidemiol Glob Health 2019; 9: 217-222.
[24] Lyon RP, Jonas M, Frantz C, Trueblood ES, Yumul R, Westendorf L, Hale CJ, Stilwell JL, Yeddula N, Snead KM, Kumar V, Patilea-Vrana GI, Klussman K and Ryan MC. SGN-B6A: a new vedotin antibody-drug conjugate directed to integrin beta-6 for multiple carcinoma indications. Mol Cancer Ther 2023; 22: 1444-1453.
[25] Peters S, Hollebecque A, Sehgal K, Lopez JS, Calvo E, Dowlati A, Bockorny B, Perez CA, Sanborn RE, Patnaik A, Fontana E, Galvao V, Kingsley E, Patilea-Vrana G, Wang T, Knowles S and Piha-Paul SA. Efficacy and safety of sigvotatug vedotin, an investigational ADC, in NSCLC: updated phase 1 results (SGNB6A-001). J Clin Oncol 2024; 42: 8521.

Lentiviral transduction of doxycycline-inducible shRNA knockdown of ITGB6

The cell lines were transduced with a doxycycline-inducible short hairpin RNA (shRNA) knockdown of αvβ6 using a lentiviral system. Both knockdown and control shRNA cell lines were pretreated with 1 μg/mL of doxycycline for five days to induce the shRNA and subsequently co-cultured with TALL-104 T-cells (Figure S1).

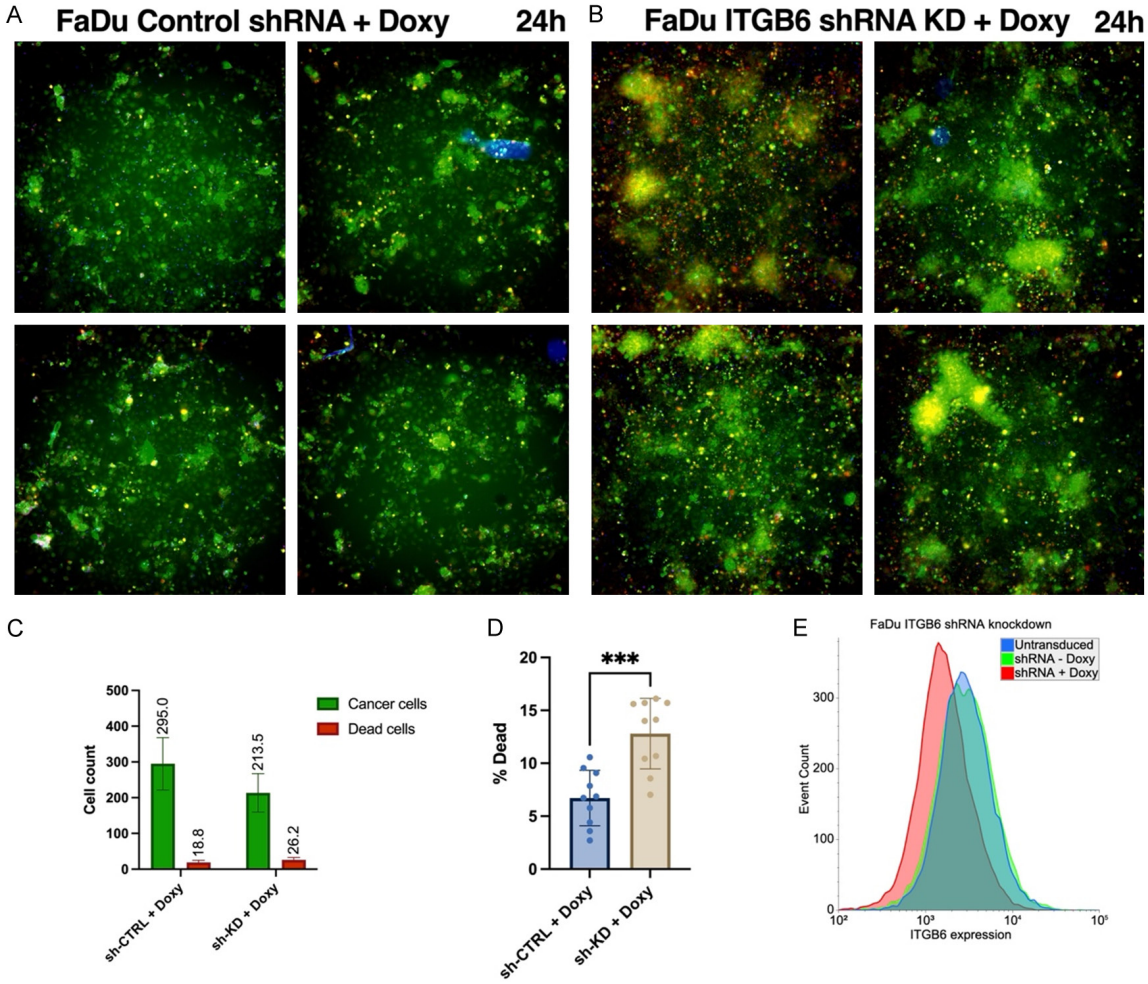

Figure S1. FaDu ITGB6 shRNA knockdown and TALL-104 co-culture. (A) Randomly chosen fields of view from co-culture of FaDu HNSCCs (green) and TALL-104 T-cells (blue). ITGB6 knockdown (KD) was initiated by pretreating either ITGB6 KD or CTRL shRNA cells (B) with 1 ug/ml Doxycycline for 72 hrs. FaDu cells were pretreated for 8 hrs with latent-TGFβ (n = 10). DNA binding cell death marker Zombie Orange (red) was added at the beginning of co-culture and the images were taken 24 hrs later. (C) Quantification of cancer cells and cancer cells exhibiting cell death marker. (D) Percentage of cancer cells exhibiting cell death marker. (E) Flow cytometry verifying doxycycline inducible knockdown of αvβ6.

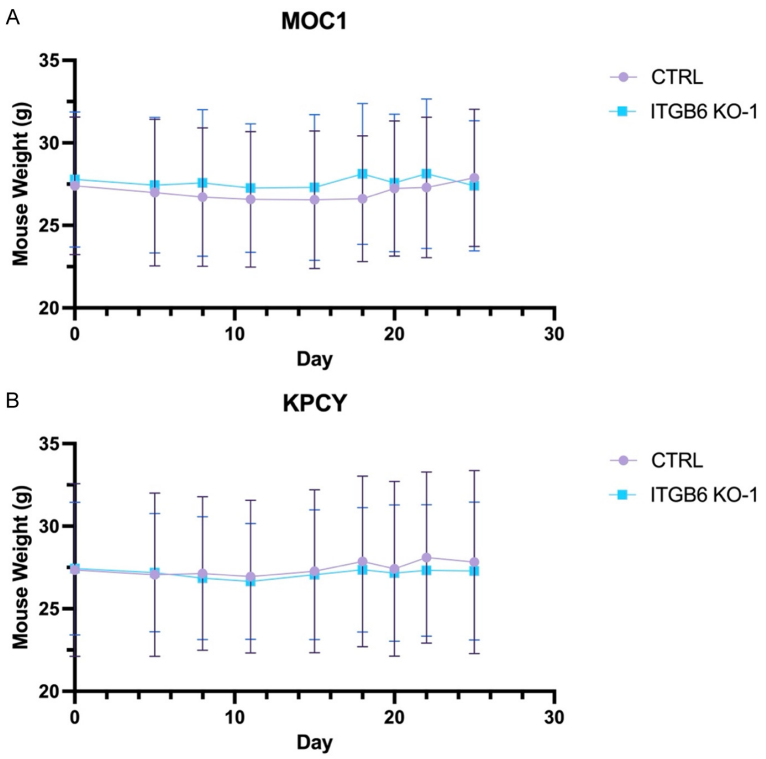

Figure S2. Weights of mice. (A) Weights of combined female and male cohorts of mice injected with MOC1 or KPCY (B) tumors with either CTRL or ITGB6 KO-1 Cas9 KO.

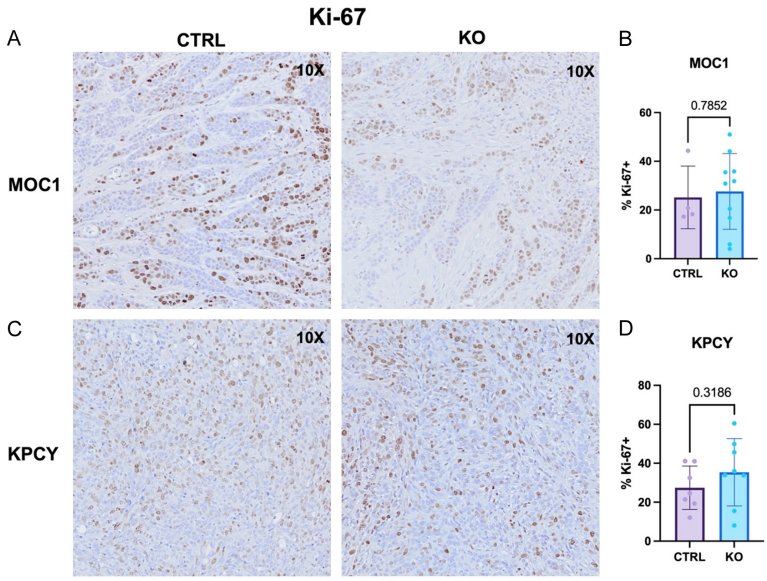

Figure S3. Ki-67 expression of mouse tumors. Representative 10X images of MOC1 (A) and KPCY (C) from scanned IHC slides showing Ki-67 expression across control and ITGB6-deficient cells. Quantification of Ki67-stained IHC slides for MOC1 (B) (control: n = 4, KO: n = 10) and KPCY (D) (control: n = 7, KO: n = 8) cohorts, showing *p*-values calculated using an unpaired t-test.